ACS APPLIED ENERGY MATERIALS

Article

Cite This: ACS Appl. Energy Mater. 2018, 1, 4522−4535

www.acsaem.org

In Situ Impedance Analysis of Oxygen Exchange on Growing $La_{0.6}Sr_{0.4}CoO_{3-\delta}$ Thin Films

Ghislain M. Rupp,* Markus Kubicek, Alexander K. Opitz, and Jürgen Fleig

Institute of Chemical Technologies and Analytics, Vienna University of Technology, Getreidemarkt 9, Vienna, AT-1060, Austria

Supporting Information

ABSTRACT: The further development of solid oxide fuel and electrolysis cells (SOFC/SOEC) strongly relies on research activities dealing with electrode materials. Recent studies showed that under operating conditions many perovskite-type oxide electrodes are prone to changes of their surface composition, leading to severe changes of their electrochemical performance. This results in a large scatter of data in literature and complicates comparison of materials. Moreover, little information is available on the potentially excellent properties of surfaces immediately after preparation, that is, before any degradation by exposure to other gas compositions or temperature changes. Here, we introduce in situ impedance spectroscopy during pulsed laser deposition (IPLD) as a new method for electrochemical analysis of mixed ionic and electronic conducting (MIEC) thin films during growth. First, this approach can truly reveal the properties of as-prepared MIEC electrode materials, since it avoids any alterations of their surface between preparation and investigation. Second, the measurements during growth give information on the thickness dependence of film properties. This technique is applied to $La_{0.6}Sr_{0.4}CoO_{3-\delta}$ (LSC), one of the most promising SOFC/SOEC oxygen electrode material. From the earliest stages of LSC film deposition on yttria-stabilized zirconia (YSZ) to a fully grown thin film of 100 nm thickness, data are gained on the oxygen exchange kinetics and the defect chemistry of LSC. A remarkable reproducibility is found in repeated film growth experiments, not only for the bulk related chemical capacitance but also for the surface related polarization resistance (±10%). Polarization resistances of as-prepared LSC films are extraordinarily low (2.0 Ω cm^2 in 40 μbar O_2 at 600 °C). LSC films on YSZ and on $La_{0.95}Sr_{0.05}Ga_{0.95}Mg_{0.05}O_{3-\delta}$ (LSGM) single crystals exhibit significantly different electrochemical properties, possibly associated with the tensile strain of LSC on LSGM.

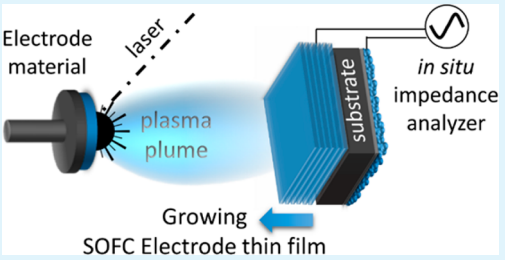

KEYWORDS: *impedance, PLD, fuel cell, SOFC, electrode, oxygen exchange, LSC, strain*

Solid oxide fuel cells (SOFCs) and solid oxide electrolysis cells (SOECs) may become important technologies to ease the transition from fossil fuels to renewable resources such as biomass and hydrogen.[1−4] Current applications include combined heating and power (CHP) systems, as well as auxiliary power units and typically operate at 700−900 °C.[5,6] The high operating temperatures restrict the choice of materials used, complicate production, decrease the durability of the components because of undesired side reactions, and therefore hamper a broad commercialization.[7] However, these challenging conditions are required for achieving sufficiently fast reaction kinetics for the oxygen incorporation or evolution at the air electrode, since reaction rates for given overpotential strongly depend on temperature (with typical activation energies in the range of 1.3−1.8 eV).[8] Hence, mixed ionic and electronic conducting (MIEC) oxides are vastly investigated in order to find, understand and design materials that offer a high catalytic activity for the oxygen exchange as well as high ionic and electronic conductivity.[9]

For SOFCs and SOECs, porous MIEC electrodes are prepared by tape casting, screen printing or dip coating to achieve electrodes with large surface area for oxygen reduction. In fundamental research, however, MIEC oxides are often prepared using pulsed laser deposition (PLD) to obtain thin films with a well-defined surface, which eases systematic studies and comparison of their catalytic activity. Thereby, different perovskite-type oxides, such as $Ba_{1-x}Sr_xCo_{1-y}Fe_yO_{3-\delta}$ (BSCF),[10−12] $La_{0.6}Ba_{0.4}CoO_{3-\delta}$ (LBC),[13] $La_{0.6}Sr_{0.4}CoO_{3-\delta}$ (LSC),[13] $La_{1-x}Sr_xCo_{1-y}Fe_yO_{3-\delta}$ (LSCF),[8,14] $La_{0.6}Sr_{0.4}FeO_{3-\delta}$ (LSF),[15] $Sm_{1-x}Sr_xCoO_{3-\delta}$ (SSC),[8] $SrFeO_{3-\delta}$ (SFO),[16] and $SrTi_{1-y}Fe_yO_{3-\delta}$ (STF),[16] have been investigated as promising cathode candidates for SOFCs. An electrode material of particular interest is LSC, since it shows very high electronic conductivity (~1000 S/cm) together with low polarization resistance for the oxygen exchange reaction (one of the lowest oxygen exchange resistances reported so far was ~0.5 Ω cm^2 for a thin film at 600 °C and 0.21 bar oxygen partial pressure[13]).

Still, LSC has yet not met all stability requirements, which not only impedes commercial application but also hampers comparability of research studies. Severe degradation of thin film electrodes, mostly related to composition changes of the

Received: April 12, 2018
Accepted: August 20, 2018
Published: August 20, 2018

DOI: 10.1021/acsaem.8b00586
ACS Appl. Energy Mater. 2018, 1, 4522−4535

thin film surface, may occur on the time scale of hours or even faster and affects reproducibility of data.[17−20] A recent study revealed that LSC surfaces might be very inhomogeneous in terms of their oxygen exchange current density, with only a few highly active, presumably Co related reaction sites in an otherwise less active Sr-terminated surface environment.[19,21] It was shown that minor surface composition changes, hardly detectable by analytical methods, had a significant impact on the oxygen exchange kinetics. These insights were gained by a novel method, which allows manipulation of the electrode surface and in situ measurement of the impedance inside a PLD chamber (IPLD).[21]

More general, tremendous performance differences by several orders of magnitude were reported in literature for LSC thin film electrodes of nominally identical composition.[13,17,19,21−32] This may be partly caused by different growth conditions, leading to nonequilibrium defects, such as grain boundaries or dislocations and possibly also to different cation stoichiometries. However, also any condition a freshly prepared PLD film is exposed to before its first characterization may contribute to these substantial differences; this includes cooling after preparation, exposure to ambient air for some time after deposition, current collector deposition or micropatterning (if required), mounting in a sample holder, heating to the measurement temperature in an atmosphere with possible impurities, etc. All these steps may modify the surface and lead to an ill-defined state of LSC (or any other) thin film electrode. Accordingly, comparability of properties found in different laboratories as well as comparability between different materials is challenging due to ill-defined pretreatments of "as-prepared" films. Also studies on the film thickness dependence of electrochemical properties and on the role of strain may be affected if changes after preparation are not avoided. This clearly indicates the need for improved methods to get reliable and reproducible data on the "virgin properties" of freshly prepared thin films.

In this contribution, we introduce such a method and directly monitor the electrochemical properties of mixed ionic electronic conducting LSC thin films during their growth in the PLD setup by using impedance spectroscopy (IPLD). This approach allows the highly reproducible analysis of the electrochemical surface polarization resistance of virgin LSC thin films during deposition. Hence, the preparation conditions during thin film growth are the only variables that may still affect the measured properties. The very low LSC surface polarization resistance obtained in these experiments also indicates a still unexploited potential of the fast oxygen exchange kinetics of LSC thin films. Equivalent circuit models are applied to determine the oxygen exchange resistance, the interfacial capacitance and the chemical capacitance of growing films, the latter revealing information on the defect chemistry. Thickness dependencies of these quantities were examined for 25 different deposition stages, starting from the earliest stages of film growth below 4 nm thickness to a fully grown thin film of 100 nm. Problems in determining accurate oxygen exchange properties for the thinnest layers are discussed. Moreover, the influence of lattice mismatch on the electrochemical film properties is studied by comparing films on yttria stabilized zirconia (YSZ) to epitaxially grown LSC on $La_{0.95}Sr_{0.05}Ga_{0.95}Mg_{0.05}O_{3-\delta}$ (LSGM) single crystals. The measured kinetic data are discussed in the context of oxygen exchange properties of LSC reported in literature.

METHODS

Sample Preparation. For most experiments (100) oriented yttria stabilized zirconia (YSZ, 9.5 mol % Y_2O_3, Crystec GmbH, Germany) single crystalline substrates were used with a thickness of 0.5 mm and a size of 5 × 5 mm^2. Some experiments were performed on (100) oriented $La_{0.95}Sr_{0.05}Ga_{0.95}Mg_{0.05}O_{3-\delta}$ (LSGM) single crystals of the same size, synthesis and preparation are detailed in ref 33. Five nm Ti (4N5; FHR Anlagenbau GmbH, Germany) and 100 nm Pt (3N5; SPM AG, Liechtenstein) thin films were deposited onto the electrolyte single crystals by a sputter coater (LS320S, Von Ardenne, Germany). Sputtering was performed at room temperature in 8 μbar Ar atmosphere. A rectangular grid structure (100 μm hole/25 μm stripe width) was then prepared on almost the entire YSZ/LSGM surface by lift-off photolithography. This Ti+Pt grid serves as current collector for the counter electrode (CE), see Figure S1a. (The thin Ti layer is used to improve adhesion of Pt to YSZ, while the electrical current collector properties are determined by the Pt layer). The sample was flipped and the process was repeated to yield another current collecting Ti+Pt grid (11/9; 35/15 or 100/25 μm hole/stripe width) over 4.5 × 4.5 mm^2 on the corresponding electrolyte surface (Figure S1b). On this grid, the LSC working electrode (WE) was deposited (see below) and its electrochemical properties were characterized by impedance spectroscopy during growth.

Targets for preparation of LSC thin films by pulsed laser deposition (PLD) were synthesized from powders prepared by a modified Pechini synthesis.[34] La_2O_3, $SrCO_3$ and Co powders (all Sigma-Aldrich, 99.995%) were individually dissolved in nitric acid, mixed in appropriate ratios and citric acid (TraceSELECT, 99.9998%) was added for chelation. After evaporation of water a viscous foam forms, which spontaneously decomposes upon further heating. The obtained intermediate product was calcined at 1000 °C, followed by isostatical pressing (~310 MPa) of the powder to a pellet and a sintering procedure at 1200 °C for 12 h in air, thus yielding a $La_{0.6}Sr_{0.4}CoO_{3-\delta}$ target for PLD. The exact film composition ($La_{0.607\pm0.008}Sr_{0.396\pm0.004}Co_{0.996\pm0.005}O_{3-\delta}$) was determined from thin films grown by standard PLD on YSZ. Those were dissolved in hydrochloric acid and analyzed by Inductively Coupled Plasma−Optical Emission Spectroscopy.

First, a microporous LSC film[22] was deposited on the CE current collector grid using PLD. Ablation of the target material was carried out by a KrF (λ = 248 nm) excimer laser (Lambda COMPexPro 201F) operated at a pulse repetition rate of 5 Hz, a pulse duration of 50 ns and a laser fluence of approximately 1.5 J·cm^{-2} at the target. The atmosphere was set to 400 μbar oxygen partial pressure O_2 and the substrate was heated to a surface temperature of approximately 450 °C. These preparation conditions lead to films with columnar structure and significant inner surface, which lead to a particularly low polarization resistance of the resulting counter electrode.[22,35] By applying 9000 laser pulses to the LSC target, a thin film of approximately 300 nm thickness was grown on the substrate (substrate to target distance = 5 cm). After deposition, the sample was cooled in the deposition atmosphere at a cooling rate of 12 °C·min^{-1} and the side faces of the YSZ crystal were gently ground to remove any residual LSC or Ti+Pt. It is noteworthy that the sample surface was never exposed to "cleaning" treatments after electrode deposition in order to avoid any contamination from solvents including H_2O.[19]

In situ Impedance PLD Measurements. The in situ impedance PLD (IPLD) setup is sketched in Figure 1a. A quartz plate is placed on top of the uncovered Pt heating wires for electronic isolation, followed by a Pt sheet, which is pinned down by a corundum plate with a 5 × 5 mm^2 opening in the center. A sample with a CE and a current collecting grid for the WE (see above) is placed into the opening such that the CE is in direct contact with the underlying Pt sheet. The sample is covered by a second corundum plate with a smaller opening (~4.2 × 4.2 mm^2) serving as a mask during PLD deposition of the working electrode. This mask is exactly center-aligned by two small corundum pegs (both corundum plates have drilled holes). Finally, the upper Ti+Pt grid, that is, the current

DOI: 10.1021/acsaem.8b00586
ACS Appl. Energy Mater. 2018, 1, 4522−4535

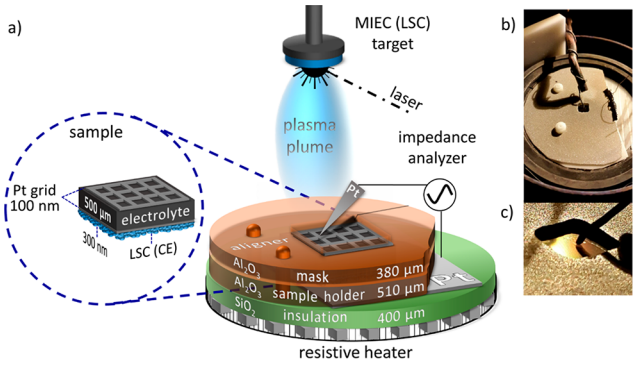

Figure 1. In situ impedance setup for PLD (IPLD): (a) Sketch of the entire setup; Ti+Pt grids (5 + 100 nm thickness) are prepared on both sides of the 5 × 5 mm^2 electrolyte single crystal (500 μm thickness) and a porous LSC counter electrode (CE) is deposited by PLD on the back side. The sample is then put on a Pt sheet on top of the PLD heater and a corundum sample holder is placed around it. Finally, a corundum mask is placed on top of the sample holder and the Pt grid is contacted by a Pt tip in the center of the sample. (b) Setup from above. (c) Pt tip contacting the Pt current collector grid; the opening of the masks is also clearly visible.

collector of the working electrode to be deposited, is contacted in the center by a Pt tip attached to a movable Cu arm, see photographs in Figure 1b and 1c. This electrical contact between Pt tip and Ti+Pt current collector grid remained intact during the entire experiment, that is, also during film deposition. The main difference compared to the IPLD setup presented in ref 21 is the use of the additional corundum masks for electronic isolation. Otherwise, deposition of a MIEC would lead to a short-circuit between WE and CE, since electrode material is not only deposited on the top but also on the outer sides of the sample.

Prior to the actual IPLD experiments, the LSC target was ground, inserted into the PLD, and ablated for 60 s at 5 Hz in 40 μbar O_2 at room temperature. Then, the PLD recipient was opened and the sample, masks and Pt tip were positioned as described above at a sample to target distance of 6 cm. Subsequently, the recipient was evacuated and the atmosphere was set to 40 μbar O_2 before heating the sample to 600 °C. The temperature was controlled by measuring the high frequency intercept in Nyquist plots of impedance measurements. At ∼600 °C this resistance is mainly caused by the ion conduction in the YSZ or LSGM single crystal, with minor contributions from the electronic sheet resistance of the Ti+Pt grid and the serial 2-point Pt wire resistance. The serial 2-point Pt wire resistance (about 2 Ω at 600 °C) was separately measured by placing the Pt tip directly on the CE Pt-sheet and the electronic sheet resistance of the Ti+Pt grid was estimated for each grid geometry according to eq S2. Hence, the temperature dependent ionic oxygen transport resistance could be determined from the measured high frequency intercept. The known conductivity−temperature relationship of our YSZ[36] and LSGM[33] single crystal electrolytes was then used to determine and control the temperature throughout the experiments (see section S-3 for more details).

The laser repetition rate was set to 1 Hz for deposition sequences of 25, 50, 100 laser pulses and increased to 2 Hz for ablations with 200, 250, or 500 laser pulses. The surface area of the WE shadowed by the contact tip during material deposition is below 4% of the total area (Figure S1c and d). This was estimated from microscope images (color contrast) after growing a complete LSC electrode (∼100 nm) on top of the YSZ single crystal. In the further analysis any substantial effect of this shadowed film region was neglected.

The impedance measurements were performed by a Novocontrol Alpha A High Performance Frequency Analyzer in the frequency range from 10^6 to a minimum of 10^{-2} Hz with a resolution of five points per decade and an alternating voltage of 10 mV (rms) applied between the WE and the CE. After each deposition sequence, up to three spectra (each taking more than 10 min of measuring time) were measured subsequently and those were generally in excellent agreement. This guarantees that any resistance and capacitance changes found after additional deposition steps are true effects, not altered by any degradation processes, and that sufficiently mobile defects, such as oxygen vacancies in the LSC thin film are equilibrated.

LSC Growth Rate. A profilometer (DekTakXT, Bruker, USA) was used to determine the LSC film thickness grown on YSZ and LSGM substrates to calculate the growth rate (pulses/nm). For this procedure about 5000 laser pulses at 2 Hz repetition rate were applied to the respective targets and the films were grown under the same PLD conditions as for the IPLD experiments (600 °C substrate temperature, 40 μbar O_2 atmosphere). Subsequently, photolithography and chemical etching were employed to remove parts of the thin films, thus generating multiple steps which could be analyzed. A nominal LSC film thickness of about 100 ± 7 nm was found for both substrates, which yields a growth rate of about 0.02 nm/laser pulse, assuming thickness independent film growth. Consequently, the amount of applied laser pulses (assuming linear film growth) was translated to a nominal film thickness for the growing LSC thin films. The PLD growth conditions are the same as in earlier studies on similar LSC films[13,19,28,33] and the corresponding films have proven to

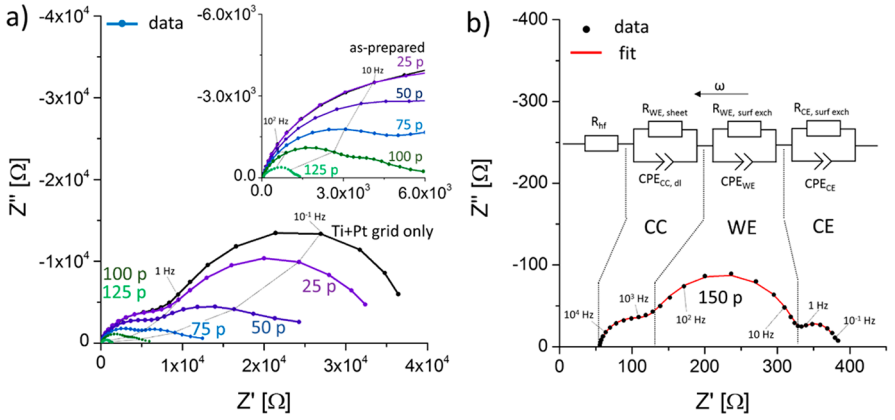

Figure 2. Impedance of a growing LSC thin film, 0−150 laser pulses (p). Representative Nyquist plots of samples with a (35/15 μm) Ti+Pt current collector grid for the top electrode. An increasing amount of LSC is then grown by applying 0−125 laser pulses onto the LSC target (25 pulses correspond to nominally 0.5 nm LSC) and impedance spectra are measured in situ at 600 °C and 40 μbar O_2 (a). After applying 150 laser pulses (nominally 3 nm LSC), the impedance spectra are primarily determined by the grown LSC thin film (see text) and the simplified equivalent circuit shown in the figure can be used to extract physically meaningful parameters (b).

DOI: 10.1021/acsaem.8b00586
ACS Appl. Energy Mater. 2018, 1, 4522−4535

Table 1. Resistive and Capacitive Values for Six 5 + 100 nm Ti+Pt Thin Film Grids of Different Geometries, Normalized to the Triple-Phase Boundary Length (TPB) or Surface Area (SA)

R_{mf}·SA [Ω cm^2]	R_{mf}·TPB [Ω cm]	C_{mf}/SA [F/cm^2]	R_{lf}·SA [Ω cm^2]	R_{lf}·TPB [Ω cm]	C_{lf}/SA [F/cm^2]
7.5 ± 1.8 × 10^2	8.3 ± 2.3 × 10^5	1.4 ± 1.1 × 10^{-4}	1.1 ± 1.0 × 10^4	1.2 ± 1.1 × 10^7	5.2 ± 0.8 × 10^{-4}

be highly crystalline and textured with preference of the (100) and (110) direction on YSZ[13,19] and epitaxial (100) growth on LSGM.[33]

Ex Situ Resistivity and Morphology Measurements. In-plane resistivity measurements of LSC thin films were performed in a separate setup. Four platinum needles were placed on LSC thin films deposited onto a 10 × 10 mm^2 YSZ single crystal close to the sample edge to meet the prerequisites of the van der Pauw method.[37] A series of LSC thin films with different nominal thicknesses (1−100 nm) was investigated. The setup was uniformly heated in a tube furnace and the temperature was measured by means of an encapsulated type K thermocouple positioned adjacent to the sample. A mixture of high purity N_2/O_2 was used to realize an oxygen partial pressure of 0.21 bar. A precision voltage source (2410, Keithley Instruments, USA) and a multimeter (2000, Keithley Instruments, USA) were employed for these conductivity measurements.

Atomic force microscopy (AFM) was performed after depositing LSC thin films onto a LSGM or YSZ substrate to analyze the different surface microstructures (Figure S3). A Nanoscope V multimode setup was utilized in tapping mode, equipped with silicon tips. In general, a scan rate of 2 Hz and a resolution of 512 × 512 pixels over a scan area of 1 × 1 μm^2 were chosen. The collected data were evaluated and plotted by Bruker's NanoScope Analysis 1.3 software.

RESULTS AND DISCUSSION

Qualitative Impedance Changes during the First Stages of LSC Film Growth. The initial sample consists of a Ti+Pt grid on top of the YSZ single crystal with a porous LSC counter electrode (CE). After mounting it in the IPLD setup (more details in Methods) and thermal equilibration at 600 °C in 40 μbar O_2 an impedance spectrum was measured, see Figures 2a and S2. The impedance is characterized by a high frequency intercept on the x-axis (>50 kHz) followed by two depressed semicircles at medium (50 kHz−1 Hz) and low (1 Hz−10 mHz) frequencies. The high frequency intercept on the real axis of the Nyquist plot (R_{hf} ∼ 55 Ω) can be largely attributed to the oxide ion conduction in the electrolyte ($R_{ion,YSZ}$ > 0.8 × R_{hf}) with small contributions from the electronic sheet resistance of the Ti+Pt grid ($R_{eon,grid}$ = ∼5−10 Ω) and the wiring resistance ($R_{eon,wire}$ = ∼2 Ω), see section S-4 for more details. This spectrum was fitted to an R_{hf} − R_{mf}||CPE$_{mf}$ − R_{lf}||CPE$_{lf}$ equivalent circuit (CPE = constant phase element), see Figure S2. Averaged fit results of six samples were normalized to the triple phase boundary (TPB) length, as well as to the surface area (SA) of the metal grid and the resulting mean values are given in Table 1.

Owing to the low polarization resistance of the CE[22,35] both arcs can be attributed to the Ti+Pt grid electrode. The TPB related low frequency resistance of the Ti+Pt grid is close to the oxygen exchange resistance expected for micropatterned Pt thin film electrodes at 600 °C in air (1.0 × 10^7 Ωcm).[36] Measured capacitances are in the range of several tens or even hundreds of μF/cm^2 in parallel to the oxygen exchange path. Comparable values have also been reported for different metal electrodes sputtered on YSZ and are usually attributed to a capacitance at the electrolyte/electrode interface.[38−41] Hence, the initial current collector grid seems to be similar to TPB active Pt electrodes on YSZ, with the resistance being due to oxygen exchange close to the TPB and the capacitance originating from the entire interfacial area. A more detailed analysis is beyond the scope of this paper, since the metal grid only acts as current collector in our experiments, at least after 3 nm of LSC were deposited, see explanation below.

Strong changes of the impedance spectra are observed when depositing small amount of LSC, see Figure 2a. The total resistance of the sample decreases by almost 2 orders of magnitude from 37.5 kΩ down to 0.4 kΩ after applying 150 laser pulses to the LSC target (i.e., for 3 nm nominal LSC film thickness), cf. Figure 2b. Moreover, the shape of the impedance spectra changes as well. The two semicircles found in the beginning become more and more depressed and uncommonly (tail-like) shaped, but after applying 150 laser pulses on the LSC target a "regularly-shaped" impedance spectrum is again found, now with three semicircles.

These observations indicate that already when depositing very small amounts of LSC a much faster oxygen exchange path becomes active. Since LSC is an electrode material with oxygen exchange proceeding via the bulk path, it is reasonable to assume that establishing this pathway upon growing the electrode is responsible for the drastic decrease of the polarization resistance. For very small pulse numbers there might still be a contribution from the current collector grid because of incomplete covering by LSC. However, after depositing about 3 nm LSC (150 pulses), the resistance has decreased to less than 1% of its original value and the transition from a TPB active metal grid electrode to a purely MIEC bulk path active LSC electrode is certainly completed. Covered by LSC, the metal grid is no longer contributing to the oxygen exchange reaction but only serves as current collector that supplies electrons to the reaction sites at the LSC surface.

The following scientific questions can therefore be addressed by further film growth and IPLD analysis:

i. What is the absolute value of the oxygen surface exchange resistance of LSC ($R_{LSC,\ surf\ exch}$) immediately after preparation?
ii. How reproducible is this value?
iii. Does the oxygen surface exchange resistance of LSC change with increasing layer thickness?
iv. Does the volume specific chemical capacitance and thus the concentration of defects depend on LSC film thickness?
v. Is there an additional interfacial contribution to the capacitance of LSC thin films?
vi. How does the surface exchange resistance and the chemical capacitance of freshly prepared LSC depend on the substrate, for example, on strain?

To answer these questions, we need to extract the corresponding resistive and capacitive parameters of LSC thin film electrodes from the impedance spectra.

Analysis of Impedance Spectra. For analyzing the spectrum measured after 150 pulses (3 nm LSC), and spectra of thicker films, we have to consider all kinetic processes involved in this experiment. First of all, we have to keep in mind that oxygen exchange on dense LSC thin film electrodes takes place via the so-called bulk path with oxygen reduction/

DOI: 10.1021/acsaem.8b00586
ACS Appl. Energy Mater. 2018, 1, 4522−4535

evolution at the surface, ion transport through the film and interfacial ion transfer from electrode into the electrolyte.[8,14] Moreover, we have to take into account that the oxygen exchange path through the LSC bulk not only requires an ionic connection to the electrolyte but also an electronic connection to the current collector grid. During the in situ growth experiment, LSC is deposited on both the Ti+Pt grid and on the electrolyte in between the metal stripes. Since, the metal grid is considered to be blocking for oxygen diffusion (see above), LSC deposited on top of the grid is virtually ionically disconnected from the electrolyte, only a very resistive ionic in-plane path to YSZ exists, provided the "side walls" of the current collector grid are also covered by LSC. Thus, practically only LSC deposited in the mesh holes of the grid and thus in direct contact with YSZ can participate in the oxygen exchange reaction.

The sketch in Figure 3 indicates the geometry of a mesh-hole cross-section after depositing some LSC and illustrates the oxygen exchange path, together with a proposed equivalent circuit. The latter is derived from the general description of mixed ionic and electronic conductors (MIEC) by Jamnik and Maier[42] (cf., also ref 43). It includes the in-plane electronic resistances of Pt ($R_{eon,Pt}$) and LSC ($R_{eon,LSC}$), the ionic resistance of YSZ ($R_{ion,YSZ}$), and the oxygen surface exchange resistance of LSC ($R_{surfexch,LSC}$). In accordance with other studies on LSC thin films the ionic across-plane transport resistance is neglected;[19,29,30] also the ionic interfacial transfer resistance between LSC and YSZ is neglected because of absence of a corresponding impedance arc in thicker films, see below.

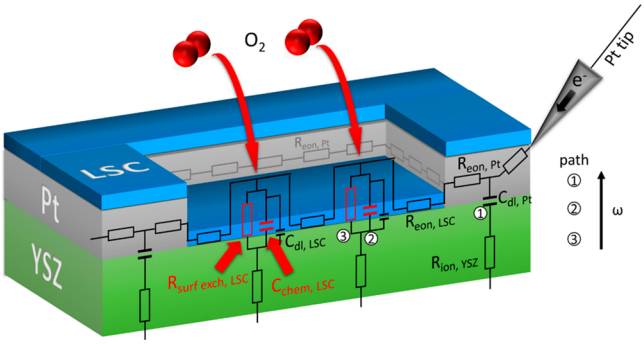

Figure 3. Mesh-hole cross-section after depositing some LSC on as-prepared samples. The oxygen exchange path is illustrated together with a 3D equivalent circuit model that allows to fully describe resistive and capacitive contribution expected after depositing >3 nm of LSC.

Capacitive behavior can originate from the interfacial capacitance between the Ti+Pt grid and YSZ ($C_{dl,Pt}$), the interfacial capacitance between LSC and YSZ ($C_{dl,LSC}$), and the chemical capacitance of the LSC bulk ($C_{chem,LSC}$). The latter two capacitances, however, are in parallel in the model of a MIEC electrode[42] and thus cannot be separated. In principle, an exact impedance model for analyzing the impedance data may thus be established. However, because of the complexity of this circuit, particularly because of the transmission lines involved, a quantitative analysis would be very challenging. Instead a simplified equivalent circuit (Figure 2b) was used to analyze the impedance spectra obtained after depositing 3 nm or more LSC. This is considered as a very reasonable approximation, provided the arcs are fairly well separated.

At high frequencies, all capacitors mentioned above exhibit low impedances and only a serial high frequency offset resistance (R_{hf}) is measured. This was already discussed above; it is dominated by the ionic resistance of YSZ but also includes the electron sheet resistance in the Pt grid and a Pt-tip contact resistance. The current can flow via path 1 sketched in Figure 3. For $C_{dl,Pt}$ being smaller than the parallel connection of the two LSC related capacitances, lower frequencies result in a current path via the two still open LSC capacitors (path 2 in Figure 3). However, then the electronic sheet resistance in the LSC comes into play and an arc results in the impedance spectrum (50 kHz−0.5 kHz). To a first approximation this switch of the current path can be described by a parallel connection of a capacitor due to $C_{dl,Pt}$ and a resistor reflecting contributions of $R_{eon,LSC}$. In the simplified circuit the corresponding arc is represented by the effective working electrode resistor $R_{WE,\ sheet}$ and a constant phase element CPE_{cc}, from which capacitances can be deduced, see below.

For even lower frequencies (0.5 kHz−1 Hz) also the LSC related capacitors achieve high impedance values, the current now takes path 3 across the oxygen exchange resistance and

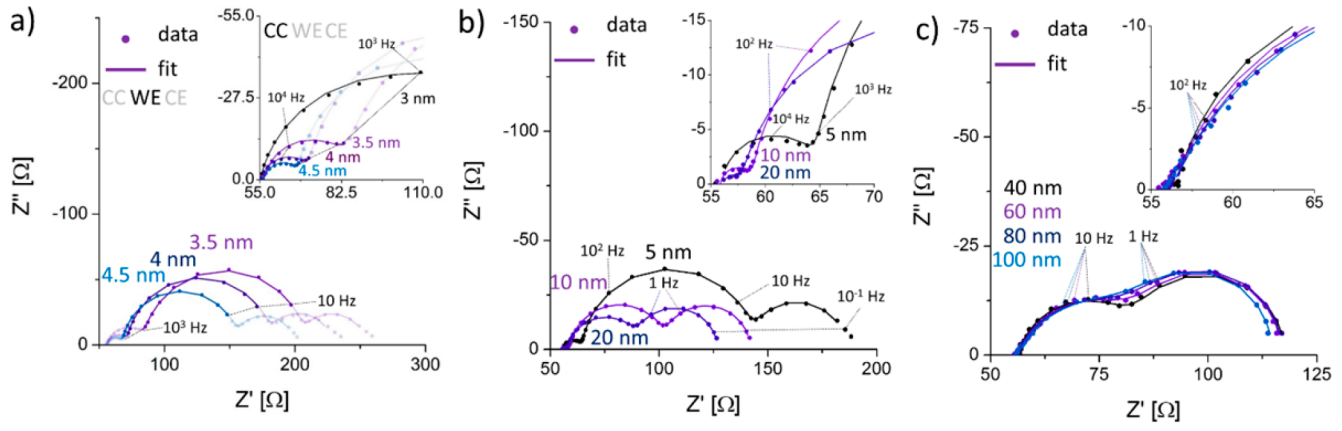

Figure 4. Impedance spectra for a growing LSC thin film, 150−5000 laser pulses, that is, 3−100 nm. Representative Nyquist plots showing the continuous growth of an LSC thin film from 3−4.5 (a), 5−20 (b), and 40−100 nm (c) on a (35/15 μm) Ti+Pt grid. The LSC thin film is grown (0.02 nm/laser pulse) and electrochemically measured in situ at 600 °C and 40 μbar O_2 by IPLD. All experimental data are fitted to the equivalent circuit shown in Figure 2b.

DOI: 10.1021/acsaem.8b00586
ACS Appl. Energy Mater. 2018, 1, 4522−4535

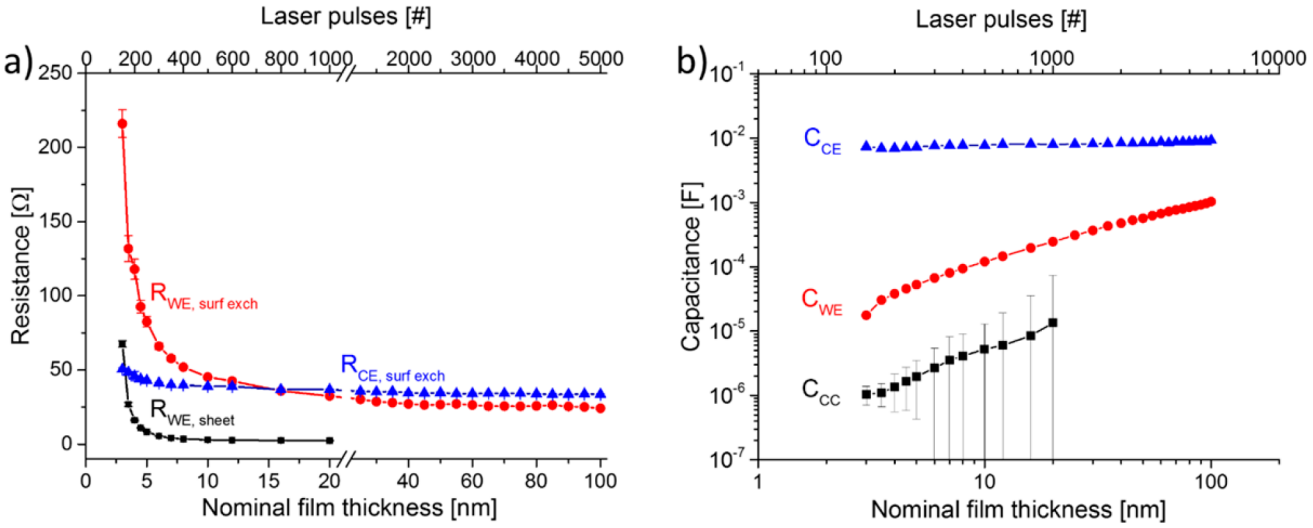

Figure 5. Resistances (a) and capacitances (b) of an LSC thin film grown and measured in situ by IPLD. The LSC thin film was deposited at 600 °C in 40 μbar O_2 on YSZ single crystal electrolyte with a (35/15 μm) current collector grid. The corresponding impedance spectra are shown in Figure 3 and 5 and values were extracted by the equivalent circuit shown in Figure 3b.

another arc results which can be approximated by the effective oxygen exchange resistance $R_{WE,surfexch}$ and CPE_{WE}. In particular, $R_{WE,surfexch}$ and C_{WE} (from CPE_{WE}) give insight into the kinetic and thermodynamic properties of our growing LSC thin film, respectively. A very similar situation was already considered in ref.[43] for a MIEC under reducing conditions. The last semicircle like feature (<1 Hz) is determined by the oxygen exchange kinetics at the counter electrode (R_{CE}), in parallel to the rather large chemical capacitance of the comparatively thick CE, represented by CPE_{CE}. All constant phase elements can be used to calculate capacitances according to ref 44 by $Z_{CPE} = Q^{-1}(i\omega)^{-n}$ and $C = (R^{1-n}\cdot Q)^{1/n}$ from fitting parameters Q and n. On the basis of this interpretation of impedance spectra, we can now quantitatively analyze the absolute values and film thickness dependences of all sample properties for LSC films beyond 3 nm thickness, i.e. LSC prepared by more than 150 pulses (next two subsections). This analysis also further illustrates the appropriateness of the suggested impedance interpretation.

Fit Parameter Changes during Further Film Growth. Figure 4 displays spectra found for LSC layers prepared by up to 5000 laser pulses, corresponding to a film thickness of about 100 nm. With continuous film growth, the diameter of the high frequency semicircle decreases until it can no longer be fitted properly for thin films with thicknesses of 20 nm or more; $R_{WE,sheet}$ in the equivalent circuit is then fixed to zero. For very thin films, the medium frequency semicircle also decreases with increasing film thickness, but then reaches a constant level for thicker films. The low frequency semicircle remains almost unaffected by the deposition of LSC, in accordance with its interpretation as the counter electrode impedance. Parameterization of the impedance spectra was done by complex nonlinear least-squares fitting using the equivalent circuit in Figure 2b and results are summarized in Figure 5a.

As already mentioned, $R_{WE,surfexch}$, strongly decreases during the first few hundred laser pulses and reaches a constant value after about 20 nm. At first sight, this seems to indicate a severe film thickness dependence of the LSC oxygen exchange kinetics. However, simultaneously $R_{WE,sheet}$ strongly decreases with increasing thickness and reaches zero for almost the same amount of laser pulses and thus layer thickness. The similar behavior of these two resistances indicates that the parameters are correlated. We first consider $R_{WE,sheet}$ in more detail.

According to our interpretation, $R_{WE,sheet}$ is primarily determined by $R_{eon,LSC}$, the electronic sheet resistance of LSC between the metal stripes, see Figure 5. For simple geometric reasons this value should indeed exhibit a decrease for increasing thickness. However, when assuming a typical electronic conductivity of LSC (1000 S/cm[13]) numerical finite element simulations (COMSOL) for the given geometrical parameters could not reproduce the absolute value of $R_{WE,sheet}$ at the beginning of the experiment. Hence, a further effect has to come into play. Additional ex situ measurements on very thin LSC films were conducted using Van der Pauw's method to measure the true in-plane conductivity (electronic conductivity), see Figure 6. A strong decrease of the nominal electronic conductivity by orders of magnitude is observed when the film thickness is reduced below a critical film thickness of about 20 nm (1000 laser pulses). This is in

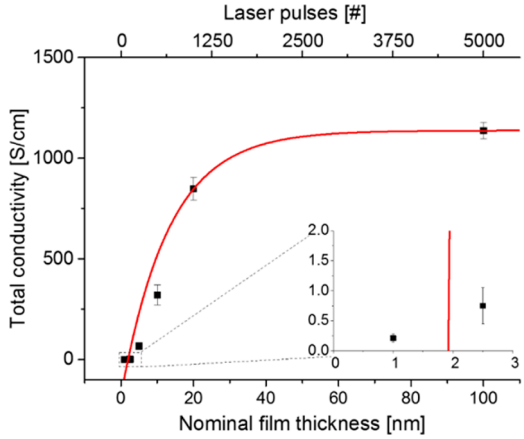

Figure 6. Total (effective) conductivity ($\sigma_{eon} \gg \sigma_{ion}$) of LSC thin films depending on the number of applied laser pulses, that is, film thickness. The conductivity was measured in van-der-Pauw geometry at 600 °C and 10 μbar $p(O_2)$. Between 50 and 5000 laser pulses were applied to a LSC target in order to grow films of 1 to 100 nm nominal thickness.

DOI: 10.1021/acsaem.8b00586
ACS Appl. Energy Mater. 2018, 1, 4522−4535

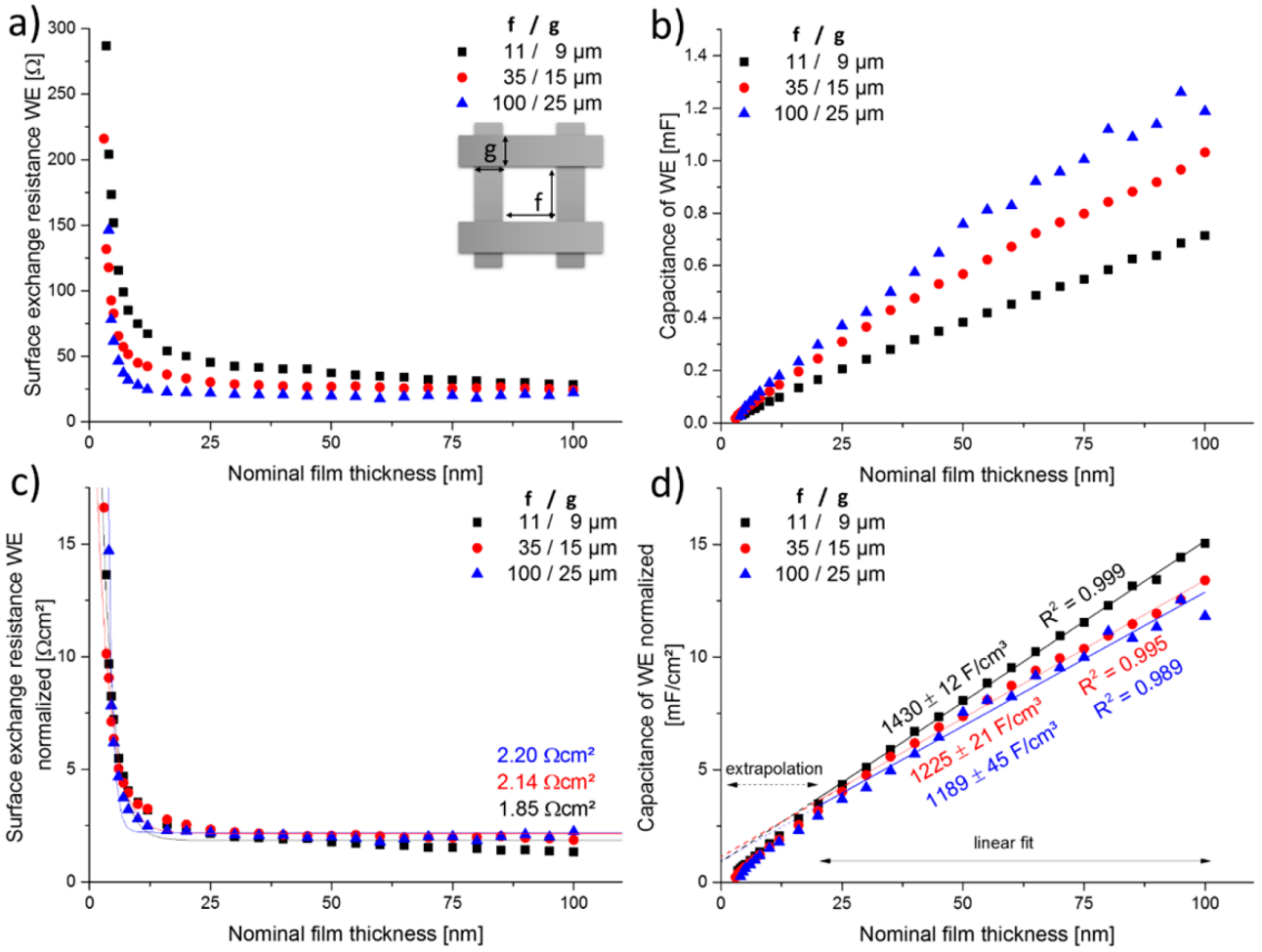

Figure 7. Resistive ($R_{WE,surf,exch}$) and capacitive (C_{WE} = $C_{chem,LSC}$ + $C_{dl,LSC}$) properties of growing thin films measured in situ by IPLD. Surface exchange resistance and capacitance of the LSC working electrode before (a, b) and after (c, d) normalization to the grid-free area, measured at 600 °C and 40 μbar O_2. Three different rectangular metal grid geometries were employed (11/9, 35/15, or 100/25 μm hole/stripe width) to verify that only LSC in direct contact with the electrolyte participates in the oxygen exchange reaction.

excellent accordance with the very pronounced increase of $R_{WE,sheet}$ below 20 nm resulting from our analysis of in situ impedance experiments. Most probably, very thin layers have a complex and possibly islands-like morphology rather than an exactly homogeneous thickness. Thus, tortuosity plays a significant role and enhances the LSC sheet resistance especially in the early stages of thin film growth.

This reduced in-plane electron conduction of very thin films directly affects $R_{WE,surfexch}$. It limits the polarized electrode area and thus only LSC close to the metal grid participates in the oxygen exchange, while LSC surface further away from the current collector remains electrochemically inactive. Therefore, a higher nominal $R_{WE,surfexch}$ can be expected as long as a significant LSC sheet resistance exists. This is exactly what we see in Figure 5a: In the beginning, $R_{WE,surfexch}$ strongly decreases with increasing thickness. The LSC surface exchange resistance reaches a constant level when $R_{WE,sheet}$ has vanished, that is, when the entire LSC area between the metal stripes is polarized and thus active for the oxygen exchange. Hence, the sharp decrease of the measured polarization resistance does not indicate much higher catalytic activity for thicker films but primarily more active surface area. We have to conclude that the area specific oxygen exchange properties of very thin LSC films (<20 nm) cannot be extracted by this analysis, due to an unknown active area. Hence, also a true change of the surface exchange properties in very thin layers (e.g., due to different surfaces) cannot be excluded. For layers thicker than 20 nm, on the other hand, the surface exchange properties are thickness independent.

Between 20 and 100 nm film thickness the capacitance C_{WE} of the working electrode increases linearly with the number of applied laser pulses. However, a significant deviation from linearity to lower capacitance values occurs for thinner films (<20 nm), which cannot be clearly seen in Figure 5b due to log−log plotting of data but is explicitly addressed in the next sections. This behavior suggests that C_{WE} is also influenced by a limited in-plane electron conduction. It is in accordance with measurements performed by Wedig et al. reporting a strong influence of the electrical sheet resistance on the chemical capacitance of $Bi_{1-x}Sr_xFeO_{3-\delta}$ thin films.[45,46] Surprisingly, C_{CC} also seems to show an increase with increasing film thickness. However, with decreasing size of the high frequency semicircle (cf., Figure 4) a significant error results from the fitting procedure (see large error bars in Figure 5b), which complicates proper evaluation and hinders a clear conclusion on its thickness (in-)dependence.

Meanwhile, the counter electrode resistive ($R_{CE,surfexch}$) and capacitive (C_{CE}) quantities (Figure 5b) remain unaffected by

DOI: 10.1021/acsaem.8b00586
ACS Appl. Energy Mater. 2018, 1, 4522−4535

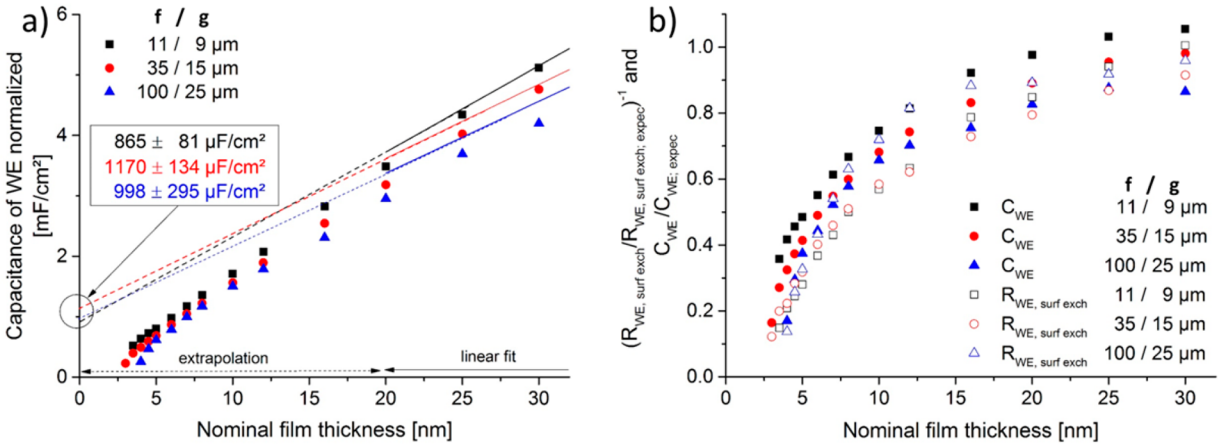

Figure 8. Capacitance of the working electrode C_{WE} (a) and of the oxygen exchange resistance as well as of C_{WE} (b) in the beginning of thin film growth. Part a is a zoom of measured data and linear fit of Figure 7d. The intersection between ordinate and the three fit lines allows determining the interfacial capacitance between LSC and YSZ. The ratios in part b reveal the similarity between deviations of resistive and capacitive properties from the values expected by extrapolation of results found for thicker layers ($R_{WE,surfexch,expec}$ = 2.02 Ω cm^2 and $C_{WE,expec}$ = 1012 µF/cm^2 + 1281 F/cm^3 × thickness).

the growth of the working electrode. Normalization to the grid-free area (0.17 cm^2) of the counter electrode, i.e. the surface that participates in the oxygen exchange, reveals a remarkably low resistance of the microporous LSC of about 5.6 Ωcm^2 at 600 °C and 40 µbar O_2.

Reproducibility and Quantitative Evaluation of the LSC Film Properties. The electrochemical LSC thin film properties, $R_{WE,surfexch}$ and C_{WE} were determined for two further thin films with different metal grid geometries. The results are shown in Figure 7a and 7b. The shape of the resistance-thickness curves for the (35/15 µm) current collector pattern is reproduced also for the other two geometries. In the beginning, a comparatively high $R_{WE,surfexch}$ is found for all grid geometries, which rapidly decreases while growing the first 10−25 nm of LSC on top. The decrease is followed by an almost ideal plateau in case of the (35/15 µm) and (100/25 µm) sample. For the LSC thin film with a very narrow grid (11/9 µm) the resistance still slightly decreases. The capacitance increases linearly for larger LSC thicknesses but exhibits a deviation from linearity with an *x*-axis offset for very thin films.

Figure 7c and 7d show the same results after normalization to the mesh hole area, that is, the area of LSC deposited directly on YSZ. For resistances as well as capacitances this leads to almost perfectly coinciding curves. This supports the assumption that indeed only LSC deposited directly on top of the electrolyte participates in the oxygen exchange and contributes to the capacitance. It also indicates the excellent reproducibility of the LSC film properties immediately after deposition. The slight drift to a lower specific resistance found with the narrow grid (11/9 µm) sample for increasing LSC thickness is most probably caused by the decreasing ionic sheet resistance above the metal current collector grid. Small parts of LSC above the metal grid and close to the LSC/YSZ interface might participate in the oxygen exchange as well and this becomes especially relevant for the finest grid. An increase of the active LSC area of a 100 nm thin film by activating a ∼500 nm wide LSC region above the current collector, that is, an effective mesh size of (12/8 µm) instead of (11/9 µm) would already lead to the same $R_{WE,surfexch}$ and C_{WE} for all mesh geometries. An estimate of the decay length of the electrochemical activity can be found in the S-6. This effect becomes less important for larger mesh widths. However, a purely empirical correction of the values for different current collectors would add some arbitrariness and the area-specific values were thus not corrected in the further analysis.

On the basis of these measurements, we can now answer questions i, ii, and iii raised above (reproducibility and absolute value of $R_{LSC,surfexch}$,as well as its thickness dependence). First, the agreement of the oxygen exchange resistances measured for different films is remarkable. When fitting the data to exponential decay functions (see lines in Figure 7c), an average oxygen exchange resistance of 2.04 ± 0.1 Ω cm^2 is determined for a fully grown thin film (>50 nm) measured at 600 °C in 40 µbar. It should be noted that most studies on LSC polarization resistances, report variations in the range of a factor of 2 or more, even for nominally identical samples.[8,26,30] The very high reproducibility found in our study can be most probably attributed to the type of experiment, with films never being exposed to other atmospheres or temperatures and being measured immediately after deposition. Second, the polarization resistance of 2.0 Ω cm^2 value is impressively low, taking into account the very low oxygen partial pressure of 40 µbar used here. A more detailed discussion of this absolute value, also comparing this low polarization resistance with other literature values, can be found below. And third, these experiments again confirm that there is no thickness dependency of $R_{WE,surfexch}$ for films larger than 20 nm thickness.

For a further analysis of the thickness dependent capacitances, C_{WE}, we first normalize the raw data (Figure 7b) to the nominally active area, that is, to the area of LSC directly on YSZ (Figure 7d). Above ∼20 nm film thickness a linear relation is found for all three experiments and a linear fit leads to very similar slopes, on average to 1281 ± 39 F/cm^3. This linearly growing contribution to C_{WE} can be attributed to the chemical capacitance of the LSC film $C_{chem,LSC}$, which is a volume property of the electrode material and given by ref 33

$$C_{chem,LSC} = 4e^2 A \cdot t \left(\frac{\partial \mu_O}{\partial c_O} \right)^{-1} \quad (1)$$

with *e* being the elementary charge, *A* and *t* the electrode surface and thickness, and c_O and μ_O the concentration and

DOI: 10.1021/acsaem.8b00586
ACS Appl. Energy Mater. 2018, 1, 4522−4535

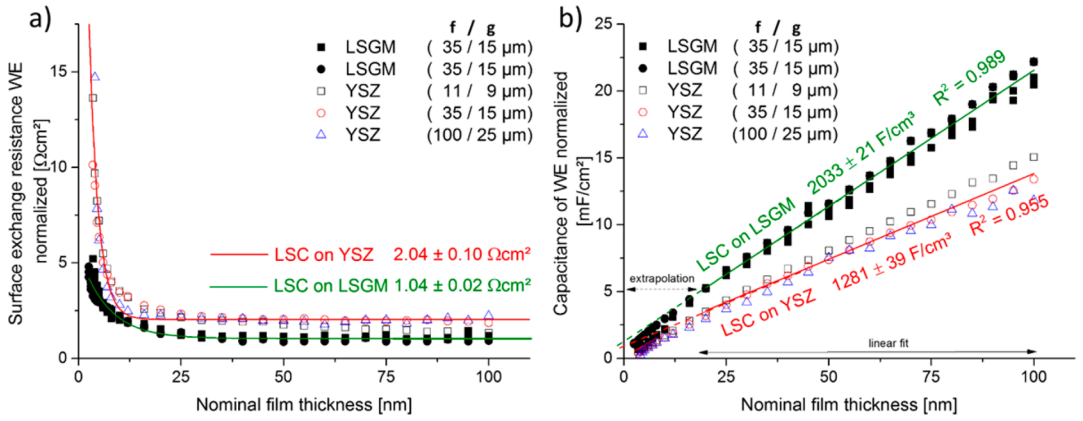

Figure 9. Resistive ($R_{WE,surf,exch}$) and capacitive ($C_{WE} = C_{chem,LSC} + C_{dl,LSC}$) properties of thin films growing on different substrates (LSGM vs YSZ) measured in situ by IPLD. Surface exchange resistance (a) and capacitance (b) of the LSC working electrode normalized to the grid-free area and measured at 600 °C in 40 μbar O_2.

chemical potential of oxygen, respectively. This identification of the main contribution of C_{WE} as the chemical bulk capacitance also justifies our interpretation of its parallel resistor $R_{WE,surfexch}$ as the oxygen surface exchange resistance: In accordance with the established models of mixed conducting electrodes,[8,14,23,29,47] only the surface related resistance is in parallel to the chemical capacitance, provided ionic bulk transport is sufficiently fast, see Figure 3. However, this surface-related resistance can include contributions from several elementary steps without leading to additional arcs in impedance spectra. Accordingly, further statements on the exact mechanistic character of $R_{WE,surfexch}$ require more detailed studies, for example, on the $p(O_2)$ and overpotential dependence.[48]

Extrapolation of the linear fits (Figure 7d) leads to an intersection with the ordinate at very similar values (1012 ± 253 μF/cm^2), see also the plot of the normalized WE capacitance for the first nanometers of thin film growth in Figure 8a. The interpolated ordinate intersect of about 1000 μF/cm^2 is interpreted as the thickness-independent interfacial capacitance, C_{dlLSC}, which is in parallel to the measured chemical capacitance of LSC. Since the chemical capacitance and the interfacial capacitance are both in parallel to our surface exchange resistance (see ref 42 and Figure 3) a discrimination is only possible based on the thickness dependency of $C_{chem,LSC}$. This analysis thus answers questions iv and v mentioned above (thickness dependence of C_{chem} and additional capacitive contribution of the interface).

If an additional interfacial resistance were present, the interfacial capacitance could be obtained from the resulting separate impedance arc. This was the case for the interfacial capacitance reported by Baumann et al.[14] (40 μF/cm^2) measured for $La_{0.6}Sr_{0.4}Co_{0.8}Fe_{0.2}O_{3-\delta}$ electrodes on YSZ electrolyte at 750 °C in air and also for a not yet interpreted capacitance (19000 μF/cm^2) found in ref 13 for $La_{0.6}Sr_{0.4}CoO_{3-\delta}$ on YSZ at 600 °C in 250 μbar $p(O_2)$. The latter showed a behavior typical for chemical capacitances, for example, $p(O_2)$ dependence. The origin of this capacitance is still unknown, but future IPLD experiments in varying $p(O_2)$ atmospheres or under DC polarization might give insights into the nature of $C_{dl,LSC}$.

For thinner films (<20 nm) not only $R_{WE,surfexch}$ but also C_{WE} deviates from model expectations, that is, from a linear fit. For C_{WE}, we find an apparent x-axis offset (instead of a y-axis offset), followed by an asymptotic increase of C_{WE}. We already concluded that for thinner films an increasing electronic sheet resistance leads to an incomplete electrode polarization. This should cause not only an increased $R_{WE,surfexch}$, but also a decreased C_{WE} compared to fully polarized layers. Such a simultaneously appearing nonideality is indeed present and becomes obvious when comparing measured and expected values of the oxygen exchange activity ($1/R_{WE,surfexch}$) and C_{WE}, see Figure 8b. There, the ratio is shown between measured $R_{WE,surfexch}$ and thickness-independent $R_{WE,surfexch,expec}$ = 2.02 Ωcm^2, as well as between C_{WE} and $C_{WE,expec}$ = 1012 μF/cm^2 + 1281 F/cm^3 × thickness [cm]. For all thin films, a very steep increase of the respective ratios is observed in the beginning, which levels out after 20−30 nm film thickness. This very similar behavior of a bulk property ($C_{chem,LSC}$) and a surface property ($R_{LSC,surfexch}$) suggests that even below 20 nm film thickness (down to 3.5 nm) most properties of LSC do not depend much on the film thickness. Rather the virtual thickness dependence of both parameters observed here is largely caused by an incomplete current collection for very thin films.

Strained LSC Thin Films on LSGM. The high reproducibility of the properties found in our IPLD measurements allows a very accurate analysis of the role of the substrate on LSC film properties (see question vi mentioned above). While growth on YSZ leads to nanocrystalline LSC layers with several orientations, (La, Sr)(Ga,Mg)$O_{3-\delta}$ (LSGM) single crystalline electrolytes allow growth of strained epitaxial LSC layers. A detailed structural and electrochemical study on $La_{0.95}Sr_{0.05}Ga_{0.95}Mg_{0.05}O_{3-\delta}$ single crystals was presented elsewhere, including growth of strained LSC film (~0.8% tensile strain at room temperature) using similar PLD conditions.[33] Qualitatively, the impedance spectra (Figure S4) obtained during LSC film growth were similar to the ones presented in Figures 2b and 4. A smaller high frequency intercept on the x-axis is found, due to a higher ionic conductivity of LSGM, followed by 2−3 arcs representing $R_{WE,sheet}$ (again only visible in the beginning of film growth), $R_{WE,surfexch}$ and $R_{CE,surfexch}$. Hence, all data could again be fitted to the equivalent circuit shown in Figure 2b and the extracted quantities for two LSC/LSGM samples are compared to the LSC/YSZ samples in Figure 9.

In accordance with the observations for LSC on YSZ, a steep decrease of $R_{WE,surfexch}$ in the beginning of film growth is also

DOI: 10.1021/acsaem.8b00586
ACS Appl. Energy Mater. 2018, 1, 4522−4535

Table 2. Oxygen Surface Exchange Resistances of Dense $La_{1-x}Sr_xCoO_{3-\delta}$ Thin Films Deposited by PLD Measured at Different Conditions by Several Authors[a]

study	electrode setup + annealed?	$La_{1-x}Sr_xCoO_{3-\delta}$ x =	substrate	measured pO_2 [bar]	measured T [°C]	measured R [Ω cm^2]	calculated R 600 °C, 0.21 bar pO_2 [Ω cm^2]
here	Macro 5 × 5 mm^2 + CC↓	0.4	LSGM	4×10^{-5}	600	1	4×10^{-3}*
here	Macro 5 × 5 mm^2 + CC↓	0.4	YSZ	4×10^{-5}	600	2	9×10^{-3}*
ref 19	Macro 5 × 5 mm^2	0.4	YSZ	1×10^{-3}	400	120	2×10^{-2}*
ref 21	Macro 5 × 5 mm^2	0.4	GDC/YSZ	4×10^{-5}	450	254	2×10^{-1}*
ref 13	Macro 5 × 5 mm^2	0.4	YSZ	0.21 syn. air	600	5×10^{-1}	5×10^{-1}
	+ 15 h annealed					42×10^{-1}	42×10^{-1}
ref 19	Macro 5 × 5 mm^2	0.4	YSZ	0.21 syn. air	600	6×10^{-1}	6×10^{-1}
	+ 15 h annealed					46×10^{-1}	46×10^{-1}
ref 17	Macro 5 × 5 mm^2	0.4	YSZ	0.21 air	600	7×10^{-1}	7×10^{-1}
	+ 72 h annealed					170×10^{-1}	170×10^{-1}
ref 22	Micro ø 0.2 mm	0.4	YSZ	0.21 air	550	2.5	9×10^{-1}
ref 28	Micro ø 0.2 mm	0.4	YSZ	0.21 air	400	200	1.2
ref 24	Macro ø 5 mm	0.5	YSZ	0.1	600	5	3.1
ref 23	Micro ø 0.2 mm	0.2	GDC/YSZ	0.1	520	50.5	5.5
ref 26	Micro ø 0.2 mm	0.4	GDC/YSZ	0.1	520	55	6
ref 27	Macro ø 10 mm	0.4	GDC Pellet	0.21 syn. air	725	1.5	13
ref 20	Macro 10 × 10 mm^2	0.2	GDC/YSZ	0.21 air	530	82	18
	+ CC↑ + 45 h annealed					1860	412
ref 31	Macro 10 × 10 mm^2 + CC↑	0.2	GDC/YSZ	0.21 air	550	65	23
ref 30	Micro ø 0.2 mm	0.2	GDC/YSZ	0.1	510	700	60
ref 25	Micro ø 0.06 − 0.1 mm	0.4	YSZ	0.21 air	750	7	88
ref 32	Micro ø 0.2 mm + 67 h annealed	0.2	GDC/YSZ	0.1	550	424	93
						20977	7337
ref 29	Macro ø 17 mm	0.4	GDC Pellet	0.1	800	45	712

[a]The term "Macro" refers to LSC thin films that were directly measured after PLD processing without current collecting thin film grid or with current collector beneath (CC↓) or after application of a thin film current collector on top (CC↑). "Micro" refers to electrode thin films, which underwent a micro-structuring step after thin film preparation. Some references include ex situ measurements of freshly prepared samples and values after annealing for given times. Asterisk (*) indicates that the pressure during measurement was much lower than 0.21 bar and thus extrapolation includes more uncertainty.

measured for LSC on LSGM, followed by a saturation for films of about 20 nm thickness. Hence, the electronic sheet resistance in the beginning of film growth is again considered to be the reason for the decrease. A lower oxygen exchange resistance of 1.04 ± 0.02 Ωcm^2 is reproducibly found for LSC on LSGM measured at 600 °C and 40 μbar O_2. This indicates enhancement of the oxygen exchange kinetics by a factor of ∼2 for LSC films on LSGM compared to films on YSZ. This may be a direct consequence of the tensile strain in LSC. Faster chemical oxygen exchange coefficients for tensile strained LSC thin films deposited on STO were already measured by XRD[49] and isotope exchange experiments.[50] Moreover, a 1.6 higher chemical capacitance is determined for LSC on LSGM (2033 ± 21 F/cm^3, Figure 9b) compared to YSZ (1281 ± 39 F/cm^3). Hence, the tensile strain seems to cause a significant increase of the "effective concentration" of oxygen vacancies that determine the chemical capacitance of LSC. The latter is in agreement with theoretical and experimental work suggesting that tensile in-plane lattice strain decreases the vacancy formation energy and thus increases the vacancy concentration.[51−53] However, also more indirect effects of the different substrates on film growth might play a role, particularly for $R_{WE,surfexch}$, such as a different surface structure and chemistry of LSC on YSZ and LSGM.

Usually, strain relaxation is expected to take place above a certain critical thickness. The expected in-plane compressive strain is comparably small (0.3% at 600 °C), calculated from lattice constants[33] and thermal expansion coefficients.[54,55] To the best of our knowledge, critical thicknesses of LSC on LSGM are not reported yet. However, $SrTiO_3$ films, another perovskite-type oxide, deposited by molecular beam epitaxy on $La_{0.7}Sr_{0.3}Al_{0.65}Ta_{0.35}O_3$ or $DyScO_3$ lead to slightly larger strain values (−0.95% and 1.09%) and studies suggest a critical thickness of 30−180 nm.[56,57] For larger strains, for example, $LaAlO_3$ deposited on $SrTiO_3$ (3.17%) by PLD, strain relaxation occurs earlier (20−50 nm).[58] In our study, neither the surface exchange resistance (Figure 9a), saturating to a constant level, nor the electrode capacitance (Figure 9b), increasing linearly with increasing film thickness, give any evidence of thickness dependent strain relaxation. Hence, the critical thickness possibly exceeds the film thicknesses used here and our entire LSC films remain slightly strained. Also in our previous XRD study of 50 nm thin LSC films on top of LSGM, or on highly strained 20 nm thin LSC films deposited on $SrTiO_3$ or $LaAlO_3$,[50] no relaxation was observed. However, the electrochemical properties found here are in contradiction to measurements reported in ref.[23] for epitaxially grown, tensile strained $La_{0.8}Sr_{0.2}CoO_{3-\delta}$ thin films deposited on GDC/YSZ. There, the oxygen exchange resistance of thinner films (20, 45, 135 nm) decreased and also significant differences of the volume specific chemical capacitance between the samples were reported (not following any thickness trend). We assume that discrepancies may come from the fact that our films were never exposed to any thermal cycling (cooling from PLD preparation temperature, heating for impedance measurement). In addition, other electrode preparation steps might induce changes of $R_{WE,surfexch}$ or C_{chem} and can thus alter comparability of different studies. Measurements in the IPLD

DOI: 10.1021/acsaem.8b00586
ACS Appl. Energy Mater. 2018, 1, 4522−4535

setup seem to be particularly suited also for electrochemical investigations of substrate effects, including effects of lattice strain.

Oxygen Surface Exchange Kinetics of LSC—A Literature Comparison. Finally, we want to assess the measured polarization resistance of a freshly prepared LSC surface in the context of existing literature data. Numerous studies already investigated the oxygen exchange kinetics of LSC, but a large discrepancy between the reported values can be found. For the sake of simplicity, we only consider supposedly dense thin films prepared by pulsed laser deposition, which reliably allows relating the measured polarization resistance to the active surface area. Further, only studies reporting oxygen exchange coefficients (k^q) or oxygen surface exchange resistances ($R_{surfexch}$) derived by electrochemical methods are considered. We also focus primarily on the values reported prior to any degradation during the measurements. However, owing to the often unknown prehistory, this does not mean that no degradation has taken place before the measurements. For comparison, also exemplary resistances of degraded samples are considered.

Three different LSC compositions ($La_{0.8}Sr_{0.2}CoO_{3-\delta}$, $La_{0.6}Sr_{0.4}CoO_{3-\delta}$, and $La_{0.5}Sr_{0.5}CoO_{3-\delta}$) are frequently investigated. Often, a higher Sr concentration is believed to accelerate the oxygen exchange kinetics at the expense of thermodynamic stability of LSC.[59] However, recent studies by Crumlin[26] and la O'[23] compared similarly prepared $La_{0.8}Sr_{0.2}CoO_{3-\delta}$ and $La_{0.6}Sr_{0.4}CoO_{3-\delta}$ thin films and did not confirm a significant kinetic difference. This might again be due to the multiple effects affecting the polarization resistance mentioned in the introduction. Any comparison of data is further complicated, because various temperatures and oxygen partial pressures were used in all studies. Hence, normalization to a reference set of thermodynamic parameters is highly beneficial and a temperature of 600 °C and an oxygen partial pressure of 0.21 bar are chosen, since these were often experimentally applied and are in a relevant range for application of LSC, for example, in solid oxide fuel cells.

Normalization of the oxygen surface exchange kinetics was performed as follows.

- Temperature: An Arrhenius-type dependence of the oxygen surface exchange kinetics was experimentally confirmed in many studies between 450 and 750 °C and activation energies of 1.26,[13] 1.3,[8,24] and 1.35[31] eV were determined for LSC thin films. A mean activation energy of 1.3 eV was chosen for extrapolation of the experimental data to the reference state.
- Oxygen partial pressure: A linear relationship in log $R_{surfexch}$ versus log $p(O_2)$ plots is often found with a negative slope m of 0.41,[27] 0.57,[24] 0.63,[23] 0.65,[13] 0.66,[30] 0.72,[26] or 0.8.[32] The meaning of this slope can be very complex and it should be emphasized that unambiguous interpretation in terms of a rate limiting reaction step is very challenging.[48,60,61] A mean negative slope of 0.63 is used to account for different oxygen partial pressures in experiments.

An overview of measured and extrapolated oxygen surface exchange resistance is given in Table 2. At a first glance, the tremendous difference of at least 3 orders of magnitude between $R_{surfexch}$ values (5×10^{-1}–712 Ωcm^2, excluding studies marked with an asterisk) obtained in different studies becomes apparent. Even if one attempts to normalize the results for each study to an individual combination of minimum and/or maximum values of the activation energy and partial pressure dependence m (mentioned above) in a way that calculated absolute $R_{surfexch}$ values move closer together, the discrepancy of 2.5–3 orders of magnitude is still found. Therefore, normalization cannot be held responsible for the large scatter.

For the sake of comparison, Table 2 also includes $R_{surf,exch}$ values of several LSC thin films deliberately degraded by annealing. An increase by 1–2 orders of magnitude already after several 10 h was found by different authors. The degradation mechanism of LSC is not fully understood yet but there is general agreement that strontium surface segregation plays a major role.[17,18,20,62] Recently, it was also found that very small changes of the LSC surface, by depositing fractions of atomic layers of different oxides on the surface, can severely change the oxygen exchange kinetics.[21] The large scatter of $R_{surfexch}$ values measured on supposedly freshly deposited LSC thin films might therefore only reflect different surface states obtained unintentionally because of (i) preparation procedures, films grown on polycrystalline or single crystalline substrates, with or without GDC buffer layers, PLD conditions (temperature, $p(O_2)$, laser fluence, substrate-target distance, cooling procedure), sample cleaning by solvents, current collector preparation on top or below, microstructuring; (ii) sample storage conditions, humidity, gas composition (e.g., with CO_2, S-containing gases), storage time; and (iii) setup for electrochemical measurements, heating procedure, purity of applied gas mixtures, possible contamination sources inside setup (including Si), temperature gradients during microelectrode measurements.

Any of these steps might alter the surface or even the microstructure of the LSC thin film and thereby its oxygen exchange kinetics. Owing to the multiple parameters involved from preparation to electrochemical characterization, which not only differ between studies but are often not deliberately chosen or unknown, it is not possible to explain the scatter of $R_{surfexch}$ by a single parameter.

Still, two general conclusions can be drawn from the studies presented in Table 1. First, avoiding additional preparation steps after thin film deposition, that is, microstructuring, current collector preparation on top, or any other steps that might risk contamination of the surface by carbon residuals, Cr or Si poisoning, SO_2 and CO_2, has a positive effect on the oxygen exchange kinetics.[63−66] Second, two ex situ studies and this in situ study (asterisks Table 1), report extraordinary low values for the (normalized) oxygen surface exchange resistance. These films do not differ in their PLD preparation parameters (and thus crystal structure) from others with much higher surface exchange resistances.[13,19] However, these samples with very active surfaces have in common that the LSC thin films were never subjected to $p(O_2)$ above 10^{-3} bar at elevated temperatures in contrast to the other films of Table 2. Differences of the oxygen exchange kinetics between ref 21 and this study, both measuring impedance inside the PLD, probably arise from the fact that the LSC thin film in ref 21 was prepared, cooled down, stored outside, remounted in the PLD and then heated to the measuring temperature. Further, ref 19 shows only a comparatively slow degradation with an $R_{surfexch}$ increase by a factor of 2 after annealing 16 h at 400 °C in 10^{-3} bar $p(O_2)$ and in the Supporting Information of ref 21 even absence of any degradation was found for a thin film annealed at 450 °C for 7 h in 4×10^{-5} bar $p(O_2)$. Although in

DOI: 10.1021/acsaem.8b00586
ACS Appl. Energy Mater. 2018, 1, 4522−4535

this study (600 °C, 4×10^{-5} bar $p(O_2)$) degradation was not deliberately measured, since further LSC was deposited every 15−30 min on top of the existing layers, it should be noted that no evidence of any degradation was found during these intervals. Therefore, a low $p(O_2)$ seems to be advantageous for realizing highly reproducible measurements without any noticeable degradation.

Mechanistic reasons behind both high catalytic activity and slow or nonexisting degradation at low $p(O_2)$ are unknown yet and a detailed understanding requires extensive further studies. However, they might be a consequence of stabilizing a less Sr-enriched LSC surface in mildly oxidizing environment. Lee et al.[67] found for Ca, Sr and Ba doped $LaMnO_3$ that higher oxygen partial pressures, 1 versus 1.3×10^{-9} bar $p(O_2)$, lead to dopant surface segregation and even formation of secondary phases above 500 °C. In accordance with this, Tselev et al.[68] deposited $La_{5/8}Ca_{3/8}MnO_3$ thin films using PLD at 6.7×10^{-5} and 2.7×10^{-5} bar $p(O_2)$ and discovered that the surface changed from an almost complete A-site termination to almost exclusive B-site termination, respectively. Owing to a possible change of a freshly prepared surface when increasing $p(O_2)$, it is also somewhat questionable whether the oxygen partial pressure dependence used for normalization (i.e., $m = 0.63$ used here) also applies to these highly active LSC thin films. The calculated surface exchange resistance in the last column of Table 1 may thus underestimate the true resistance in air. Further investigations of the oxygen partial pressure dependence inside the IPLD setup have to at which stage LSC surfaces lose parts of their high catalytic activity and in combination with chemical analysis might reveal key processes of performance changes.

CONCLUSIONS

A novel method is introduced to characterize the electrochemical properties of freshly prepared as well as growing MIEC thin film electrodes by in situ impedance spectroscopy during pulsed laser deposition. Thin film growth and electrochemical characterization of LSC thin film electrodes are performed simultaneously, that is, under the same conditions, and this allows to monitor kinetic and thermodynamic film properties also for early stages of film growth. On the basis of a simplified equivalent circuit the electrochemical film properties (oxygen surface exchange resistance, chemical and interfacial capacitance) can be successfully extracted. The metallic current collector grid, prepared on top of the electrolyte prior to film deposition to ensure homogeneous film polarization, affects the oxygen exchange only in the very beginning of LSC film growth (up to 3 nm LSC). However, during the first 20 nm of LSC growth, a decreasing electronic sheet resistance still limits the active electrode area to parts close to the current collector grid.

Above a film thickness of 20 nm, a thickness independent oxygen surface exchange resistance of 2.04 ± 0.1 Ωcm^2 is obtained at 600 °C and 40 μbar O_2 for LSC grown on YSZ. The thickness dependence of the electrode capacitance indicates an interfacial contribution of 1012 ± 253 $\mu F/cm^2$ and a thickness independent volumetric chemical capacitance of 1281 ± 39 F/cm^3. The reproducibility of these values was very high, that is, relative errors are unusually low. These experiments thus allow determining the electrochemical properties of freshly prepared MIEC films before exposure to any change of temperature or gas atmosphere. The measured oxygen exchange resistance of such freshly prepared LSC surfaces is impressively low, taking into account that it refers to an oxygen partial pressure 5000 times smaller than in ambient air. A literature review of polarization resistance of LSC films revealed tremendous scatter, but also showed that in usual ex situ measurements most LSC films did not reach such a low polarization resistance even for oxygen partial pressures as high as 0.2 bar. Freshly prepared LSC films never exposed to temperatures, oxygen partial pressures and gases other than those used during deposition thus seem to be electrochemically extremely active.

The excellent reproducibility of the measurements also allowed investigation of the influence of comparatively small lattice mismatch (~0.3% at 600 °C) in LSC thin films grown on LSGM single crystals. An enhancement of the oxygen exchange kinetics by a factor of 2 was found for strained LSC films on LSGM compared to unstrained films on YSZ. Moreover, a higher chemical capacitance of 2033 ± 21 F/cm^3 was obtained, suggesting a decrease of the oxygen vacancy formation energy for tensile strained MIEC thin films leading to higher oxygen vacancy concentrations.

ASSOCIATED CONTENT

Supporting Information

The Supporting Information is available free of charge on the ACS Publications website at DOI: 10.1021/acsaem.8b00586.

Microscope and AFM images of the MIEC samples, details on temperature measurement and temperature control during IPLD experiments, estimate of the decay length of electrochemical activity, and impedance spectra of LSC films grown on LSGM (PDF)

AUTHOR INFORMATION

Corresponding Author

*E-mail: ghislain.rupp@tuwien.ac.at.

ORCID

Ghislain M. Rupp: 0000-0002-9241-3923
Markus Kubicek: 0000-0001-6623-9805
Alexander K. Opitz: 0000-0002-2567-1885

Notes

The authors declare no competing financial interest.

ACKNOWLEDGMENTS

The authors acknowledge funding by Austrian Science Fund (FWF) project F4509-N16 and W1243-N16. M. Glowacki from the Polish Academy of Science is gratefully acknowledged for providing the LSGM single crystal used in this study. Further, the authors like to thank G. Friedbacher for performing the AFM measurements as well as K. Hradil and W. Artner from the X-ray Center of the Vienna University of Technology for their continuous advice and support.

REFERENCES

(1) Stambouli, A. B.; Traversa, E. Solid Oxide Fuel Cells (SOFCs): A Review of an Environmentally Clean and Efficient Source of Energy. *Renewable Sustainable Energy Rev.* **2002**, *6*, 433−455.

(2) Wachsman, E. D.; Marlowe, C. A.; Lee, K. T. Role of Solid Oxide Fuel Cells in a Balanced Energy Strategy. *Energy Environ. Sci.* **2012**, *5*, 5498−5509.

(3) Choudhury, A.; Chandra, H.; Arora, A. Application of Solid Oxide Fuel Cell Technology for Power Generation—A Review. *Renewable Sustainable Energy Rev.* **2013**, *20*, 430−442.

DOI: 10.1021/acsaem.8b00586
ACS Appl. Energy Mater. 2018, 1, 4522−4535

(4) Mahato, N.; Banerjee, A.; Gupta, A.; Omar, S.; Balani, K. Progress in Material Selection for Solid Oxide Fuel Cell Technology: A Review. *Prog. Mater. Sci.* **2015**, *72*, 141−337.
(5) Ellamla, H. R.; Staffell, I.; Bujlo, P.; Pollet, B. G.; Pasupathi, S. Current Status of Fuel Cell Based Combined Heat and Power Systems for Residential Sector. *J. Power Sources* **2015**, *293*, 312−328.
(6) Wachsman, E.; Ishihara, T.; Kilner, J. Low-Temperature Solid Oxide Fuel Cells. *MRS Bull.* **2014**, *39*, 773−779.
(7) Wachsman, E. D.; Lee, K. T. Lowering the Temperature of Solid Oxide Fuel Cells. *Science* **2011**, *334*, 935−939.
(8) Baumann, F. S.; Fleig, J.; Cristiani, G.; Stuhlhofer, B.; Habermeier, H.-U.; Maier, J. Quantitative Comparison of Mixed Conducting SOFC Cathode Materials by Means of Thin Film Model Electrodes. *J. Electrochem. Soc.* **2007**, *154*, B931−B941.
(9) Sun, C.; Hui, R.; Roller, J. Cathode Materials for Solid Oxide Fuel Cells: A Review. *J. Solid State Electrochem.* **2010**, *14*, 1125−1144.
(10) Baumann, F. S.; Fleig, J.; Habermeier, H. U.; Maier, J. $Ba_{0.5}Sr_{0.5}Co_{0.8}Fe_{0.2}O_{3-\delta}$ Thin Film Microelectrodes Investigated by Impedance Spectroscopy. *Solid State Ionics* **2006**, *177*, 3187−3191.
(11) Burriel, M.; Niedrig, C.; Menesklou, W.; Wagner, S. F.; Santiso, J.; Ivers-Tiffée, E. BSCF Epitaxial Thin Films: Electrical Transport and Oxygen Surface Exchange. *Solid State Ionics* **2010**, *181*, 602−608.
(12) Wang, L.; Merkle, R.; Cristiani, G.; Stuhlhofer, B.; Habermeier, H.-U.; Maier, J. PLD-deposited $(Ba_xSr_{1-x})(Co_yFe_{1-y})O_{3-\delta}$ Thin-Film Microelectrodes: Structure Aspects and Oxygen Incorporation Kinetics. *ECS Trans.* **2008**, *13*, 85−95.
(13) Rupp, G. M.; Schmid, A.; Nenning, A.; Fleig, J. The Superior Properties of $La_{0.6}Ba_{0.4}CoO_{3-\delta}$ Thin Film Electrodes for Oxygen Exchange in Comparison to $La_{0.6}Sr_{0.4}CoO_{3-\delta}$. *J. Electrochem. Soc.* **2016**, *163*, F564−F573.
(14) Baumann, F. S.; Fleig, J.; Habermeier, H.; Maier, J. Impedance Spectroscopic Study on well-defined $(La,Sr)(Co,Fe)O_{3-\delta}$ Model Electrodes. *Solid State Ionics* **2006**, *177*, 1071−1081.
(15) Kogler, S.; Nenning, A.; Rupp, G. M.; Opitz, A. K.; Fleig, J. Comparison of Electrochemical Properties of $La_{0.6}Sr_{0.4}FeO_{3-\delta}$ Thin Film Electrodes: Oxidizing vs. Reducing Conditions. *J. Electrochem. Soc.* **2015**, *162*, F317−F326.
(16) Jung, W.; Tuller, H. L. Investigation of Cathode Kinetics in SOFC: Model Thin Film $SrTi_{1-x}Fe_xO_{3-\delta}$ Mixed Conducting Oxides. *ECS Trans.* **2011**, *35*, 2129−2136.
(17) Cai, Z.; Kubicek, M.; Fleig, J.; Yildiz, B. Chemical Heterogeneities on $La_{0.6}Sr_{0.4}CoO_{3-\delta}$ Thin Films—Correlations to Cathode Surface Activity and Stability. *Chem. Mater.* **2012**, *24*, 1116−1127.
(18) Kubicek, M.; Limbeck, A.; Fromling, T.; Hutter, H.; Fleig, J. Relationship Between Cation Segregation and the Electrochemical Oxygen Reduction Kinetics of $La_{0.6}Sr_{0.4}CoO_{3-\delta}$ Thin Film Electrodes. *J. Electrochem. Soc.* **2011**, *158*, B727−B734.
(19) Rupp, G. M.; Tellez, H.; Druce, J.; Limbeck, A.; Ishihara, T.; Kilner, J.; Fleig, J. Surface Chemistry of $La_{0.6}Sr_{0.4}CoO_{3-\delta}$ Thin Films and its Impact on the Oxygen Surface Exchange Resistance. *J. Mater. Chem. A* **2015**, *3*, 22759−22769.
(20) Tsvetkov, N.; Lu, Q.; Sun, L.; Crumlin, E. J.; Yildiz, B. Improved Chemical and Electrochemical Stability of Perovskite Oxides with less Reducible Cations at the Surface. *Nat. Mater.* **2016**, *15*, 1010−1016.
(21) Rupp, G. M.; Opitz, A. K.; Nenning, A.; Limbeck, A.; Fleig, J. Real-time Impedance Monitoring of Oxygen Reduction during Surface Modification of Thin Film Cathodes. *Nat. Mater.* **2017**, *16*, 640−645.
(22) Rupp, G. M.; Limbeck, A.; Kubicek, M.; Penn, A.; Stoger-Pollach, M.; Friedbacher, G.; Fleig, J. Correlating Surface Cation Composition and Thin Film Microstructure with the Electrochemical Performance of Lanthanum Strontium Cobaltite (LSC) Electrodes. *J. Mater. Chem. A* **2014**, *2*, 7099−7108.
(23) La O, G. J.; Ahn, S.-J.; Crumlin, E.; Orikasa, Y.; Biegalski, M. D.; Christen, H. M.; Shao-Horn, Y. Catalytic Activity Enhancement for Oxygen Reduction on Epitaxial Perovskite Thin Films for Solid-Oxide Fuel Cells. *Angew. Chem., Int. Ed.* **2010**, *49*, 5344−5347.
(24) Yang, Y. L.; Chen, C. L.; Chen, S. Y.; Chu, C. W.; Jacobson, A. J. Impedance Studies of Oxygen Exchange on Dense Thin Film Electrodes of $La_{0.5}Sr_{0.5}CoO_{3-\delta}$. *J. Electrochem. Soc.* **2000**, *147*, 4001−4007.
(25) Baumann, F. S.; Maier, J.; Fleig, J. The Polarization Resistance of Mixed Conducting SOFC Cathodes: A Comparative Study using Thin Film Model Electrodes. *Solid State Ionics* **2008**, *179*, 1198−1204.
(26) Crumlin, E. J.; Ahn, S.-J.; Lee, D.; Mutoro, E.; Biegalski, M. D.; Christen, H. M.; Shao-Horn, Y. Oxygen Electrocatalysis on Epitaxial $La_{0.6}Sr_{0.4}CoO_{3-\delta}$ Perovskite Thin Films for Solid Oxide Fuel Cells. *J. Electrochem. Soc.* **2012**, *159*, F219−F225.
(27) Wilson, J. R.; Sase, M.; Kawada, T.; Adler, S. B. Measurement of Oxygen Exchange Kinetics on Thin-Film $La_{0.6}Sr_{0.4}CoO_{3-\delta}$ Using Nonlinear Electrochemical Impedance Spectroscopy. *Electrochem. Solid-State Lett.* **2007**, *10*, B81−B86.
(28) Kubicek, M.; Huber, T. M.; Welzl, A.; Penn, A.; Rupp, G. M.; Bernardi, J.; Stöger-Pollach, M.; Hutter, H.; Fleig, J. Electrochemical Properties of $La_{0.6}Sr_{0.4}CoO_{3-\delta}$ Thin Films investigated by Complementary Impedance Spectroscopy and Isotope Exchange Depth Profiling. *Solid State Ionics* **2014**, *256*, 38−44.
(29) Kawada, T.; Suzuki, J.; Sase, M.; Kaimai, A.; Yashiro, K.; Nigara, Y.; Mizusaki, J.; Kawamura, K.; Yugami, H. Determination of Oxygen Vacancy Concentration in a Thin Film of $La_{0.6}Sr_{0.4}CoO_{3-\delta}$ by an Electrochemical Method. *J. Electrochem. Soc.* **2002**, *149*, E252−E259.
(30) Mutoro, E.; Crumlin, E. J.; Biegalski, M. D.; Christen, H. M.; Shao-Horn, Y. Enhanced Oxygen Reduction Activity on Surface-Decorated Perovskite Thin Films for Solid Oxide Fuel Cells. *Energy Environ. Sci.* **2011**, *4*, 3689−3696.
(31) Ma, W.; Kim, J. J.; Tsvetkov, N.; Daio, T.; Kuru, Y.; Cai, Z.; Chen, Y.; Sasaki, K.; Tuller, H. L.; Yildiz, B. Vertically Aligned Nanocomposite $La_{0.8}Sr_{0.2}CoO_3/(La_{0.5}Sr_{0.5})_2CoO_4$ Cathodes−Electronic Structure, Surface Chemistry and Oxygen Reduction Kinetics. *J. Mater. Chem. A* **2015**, *3*, 207−219.
(32) Lee, D.; Lee, Y.-L.; Grimaud, A.; Hong, W. T.; Biegalski, M. D.; Morgan, D.; Shao-Horn, Y. Enhanced Oxygen Surface Exchange Kinetics and Stability on Epitaxial $La_{0.8}Sr_{0.2}CoO_{3-\delta}$ Thin Films by $La_{0.8}Sr_{0.2}MnO_{3-\delta}$ Decoration. *J. Phys. Chem. C* **2014**, *118*, 14326−14334.
(33) Rupp, G. M.; Glowacki, M.; Fleig, J. Electronic and Ionic Conductivity of $La_{0.95}Sr_{0.05}Ga_{0.95}Mg_{0.05}O_{3-\delta}$ (LSGM) Single Crystals. *J. Electrochem. Soc.* **2016**, *163*, F1189−F1197.
(34) Pechini, M. P. (Sprague Electric Co.) Method of Preparing Lead and Alkaline Earth Titanates and Niobates and Coating Method Using the Same to Form a Capacitor. U.S. Patent US3330697A, 1967.
(35) Januschewsky, J.; Ahrens, M.; Opitz, A. K.; Kubel, F.; Fleig, J. Optimized $La_{0.6}Sr_{0.4}CoO_{3-\delta}$ Thin-Film Electrodes with Extremely Fast Oxygen-Reduction Kinetics. *Adv. Funct. Mater.* **2009**, *19*, 3151−3156.
(36) Opitz, A. K.; Fleig, J. Investigation of O_2 Reduction on Pt/YSZ by Means of Thin Film Microelectrodes: The Geometry Dependence of the Electrode Impedance. *Solid State Ionics* **2010**, *181*, 684−693.
(37) van der Pauw, L. J. A Method of Measuring Specific Resistivity and Hall Effect of Discs of Arbitrary Shape. *Philips Res. Rep.* **1958**, *13*, 1−9.
(38) Baker, R.; Guindet, J.; Kleitz, M. Classification Criteria for Solid Oxide Fuel Cell Electrode Materials. *J. Electrochem. Soc.* **1997**, *144*, 2427−2432.
(39) Hendriks, M. G. H. M.; ten Elshof, J. E.; Bouwmeester, H. J. M.; Verweij, H. The Electrochemical Double-Layer Capacitance of Yttria-stabilised Zirconia. *Solid State Ionics* **2002**, *146*, 211−217.
(40) Kek, D.; Mogensen, M.; Pejovnik, S. A Study of Metal (Ni, Pt, Au)/Yttria-stabilized Zirconia Interface in Hydrogen Atmosphere at elevated Temperature. *J. Electrochem. Soc.* **2001**, *148*, A878−A886.
(41) Velle, O. J.; Norby, T.; Kofstad, P. The Electrode System O_2Pt ‖ ZrO_2: $8Y_2O_3$ investigated by Impedence Spectroscopy. *Solid State Ionics* **1991**, *47*, 161−167.

DOI: 10.1021/acsaem.8b00586
ACS Appl. Energy Mater. 2018, 1, 4522−4535

(42) Jamnik, J.; Maier, J. Generalised Equivalent Circuits for Mass and Charge Transport: Chemical Capacitance and its Implications. *Phys. Chem. Chem. Phys.* **2001**, *3*, 1668−1678.
(43) Nenning, A.; Opitz, A. K.; Huber, T. M.; Fleig, J. A Novel approach for Analyzing Electrochemical Properties of Mixed Conducting Solid Oxide Fuel Cell Anode Materials by Impedance Spectroscopy. *Phys. Chem. Chem. Phys.* **2014**, *16*, 22321−22336.
(44) Fleig, J. The Grain Boundary Impedance of Random Microstructures: Numerical Simulations and Implications for the Analysis of Experimental Data. *Solid State Ionics* **2002**, *150*, 181−193.
(45) Wedig, A.; Merkle, R.; Stuhlhofer, B.; Habermeier, H.-U.; Maier, J.; Heifets, E. Fast Oxygen Exchange Kinetics of Pore-free $Bi_{1-x}Sr_xFeO_{3-\delta}$ Thin Films. *Phys. Chem. Chem. Phys.* **2011**, *13*, 16530−16533.
(46) Wedig, A.; Lynch, M. E.; Merkle, R.; Maier, J.; Liu, M. Sheet Resistance in Thin Film Solid Oxide Fuel Cell Model Cathodes: A Case Study on Circular $Bi_{1-x}Sr_xFeO_{3-\delta}$ Microelectrodes. *ECS Trans.* **2012**, *45*, 213−224.
(47) Jung, W.; Tuller, H. L. A New Model Describing Solid Oxide Fuel Cell Cathode Kinetics: Model Thin Film $SrTi_{1-x}Fe_xO_{3-\delta}$ Mixed Conducting Oxides−a Case Study. *Adv. Energy Mater.* **2011**, *1*, 1184−1191.
(48) Schmid, A.; Rupp, G. M.; Fleig, J. How To Get Mechanistic Information from Partial Pressure-Dependent Current−Voltage Measurements of Oxygen Exchange on Mixed Conducting Electrodes. *Chem. Mater.* **2018**, *30*, 4242−4252.
(49) Moreno, R.; Zapata, J.; Roqueta, J.; Bagués, N.; Santiso, J. Chemical Strain and Oxidation-Reduction Kinetics of Epitaxial Thin Films of Mixed Ionic-Electronic Conducting Oxides Determined by X-Ray Diffraction. *J. Electrochem. Soc.* **2014**, *161*, F3046−F3051.
(50) Kubicek, M.; Cai, Z.; Ma, W.; Yildiz, B.; Hutter, H.; Fleig, J. Tensile Lattice Strain Accelerates Oxygen Surface Exchange and Diffusion in $La_{1-x}Sr_xCoO_{3-\delta}$ Thin Films. *ACS Nano* **2013**, *7*, 3276−3286.
(51) Donner, W.; Chen, C.; Liu, M.; Jacobson, A. J.; Lee, Y.-L.; Gadre, M.; Morgan, D. Epitaxial Strain-Induced Chemical Ordering in $La_{0.5}Sr_{0.5}CoO_{3-\delta}$ Films on $SrTiO_3$. *Chem. Mater.* **2011**, *23*, 984−988.
(52) Kushima, A.; Yip, S.; Yildiz, B. Competing Strain Effects in Reactivity of $LaCoO_3$ with Oxygen. *Phys. Rev. B: Condens. Matter Mater. Phys.* **2010**, *82*, 115435.
(53) Cai, Z.; Kuru, Y.; Han, J. W.; Chen, Y.; Yildiz, B. Surface Electronic Structure Transitions at High Temperature on Perovskite Oxides: The Case of Strained $La_{0.8}Sr_{0.2}CoO_3$ Thin Films. *J. Am. Chem. Soc.* **2011**, *133*, 17696−17704.
(54) Vasylechko, L.; Vashook, V.; Savytskii, D.; Senyshyn, A.; Niewa, R.; Knapp, M.; Ullmann, H.; Berkowski, M.; Matkovskii, A.; Bismayer, U. Crystal structure, Thermal Expansion and Conductivity of Anisotropic $La_{1-x}Sr_xGa_{1-2x}Mg_{2x}O_{3-y}$ (x = 0.05, 0.1) Single Crystals. *J. Solid State Chem.* **2003**, *172*, 396−411.
(55) Ullmann, H.; Trofimenko, N.; Tietz, F.; Stöver, D.; Ahmad-Khanlou, A. Correlation between Thermal Expansion and Oxide Ion Transport in Mixed Conducting Perovskite-type Oxides for SOFC Cathodes. *Solid State Ionics* **2000**, *138*, 79−90.
(56) Wang, T.; Ganguly, K.; Marshall, P.; Xu, P.; Jalan, B. *Appl. Phys. Lett.* **2013**, *103*, 212904−212904.
(57) Biegalski, M.; Fong, D.; Eastman, J.; Fuoss, P.; Streiffer, S.; Heeg, T.; Schubert, J.; Tian, W.; Nelson, C.; Pan, X.; et al. Critical Thickness of High Structural Quality $SrTiO_3$ Films Grown on Orthorhombic (101) $DyScO_3$. *J. Appl. Phys.* **2008**, *104*, 114109.
(58) Liu, G.; Lei, Q.; Wolak, M. A.; Li, Q.; Chen, L.-Q.; Winkler, C.; Sloppy, J.; Taheri, M. L.; Xi, X. Epitaxial Strain and its Relaxation at the $LaAlO_3/SrTiO_3$ Interface. *J. Appl. Phys.* **2016**, *120*, 085302.
(59) Egger, A.; Bucher, E.; Yang, M.; Sitte, W. Comparison of Oxygen Exchange Kinetics of the IT-SOFC Cathode Materials $La_{0.5}Sr_{0.5}CoO_{3-\delta}$ and $La_{0.6}Sr_{0.4}CoO_{3-\delta}$. *Solid State Ionics* **2012**, *225*, 55−60.
(60) Guan, Z.; Chen, D.; Chueh, W. C. Analyzing the Dependence of Oxygen Incorporation Current Density on Overpotential and Oxygen Partial Pressure in Mixed Conducting Oxide Electrodes. *Phys. Chem. Chem. Phys.* **2017**, *19*, 23414−23424.
(61) Fleig, J.; Rupp, G. M.; Nenning, A.; Schmid, A. Towards an Improved Understanding of Electrochemical Oxygen Exchange Reactions on Mixed Conducting Oxides. *ECS Trans.* **2017**, *77*, 93−108.
(62) Hjalmarsson, P.; Søgaard, M.; Mogensen, M. Electrochemical Performance and Degradation of $(La_{0.6}Sr_{0.4})_{0.99}CoO_{3-\delta}$ as Porous SOFC-Cathode. *Solid State Ionics* **2008**, *179*, 1422−1426.
(63) Bucher, E.; Gspan, C.; Hofer, F.; Sitte, W. Sulphur Poisoning of the SOFC Cathode Material $La_{0.6}Sr_{0.4}CoO_{3-\delta}$. *Solid State Ionics* **2013**, *238*, 15−23.
(64) Bucher, E.; Gspan, C.; Hofer, F.; Sitte, W. Post-Test Analysis of Silicon Poisoning and Phase Decomposition in the SOFC Cathode Material $La_{0.58}Sr_{0.4}Co_{0.2}Fe_{0.8}O_{3-\delta}$ by Transmission Electron Microscopy. *Solid State Ionics* **2013**, *230*, 7−11.
(65) Bucher, E.; Yang, M.; Sitte, W. In Situ Investigations of the Chromium-Induced Degradation of the Oxygen Surface Exchange Kinetics of IT-SOFC Cathode Materials $La_{0.6}Sr_{0.4}CoO_{3-\delta}$ and $La_{0.58}Sr_{0.4}Co_{0.2}Fe_{0.8}O_{3-\delta}$. *J. Electrochem. Soc.* **2012**, *159*, B592−B596.
(66) Yu, Y.; Luo, H.; Cetin, D.; Lin, X.; Ludwig, K.; Pal, U.; Gopalan, S.; Basu, S. Effect of Atmospheric CO_2 on Surface Segregation and Phase Formation in $La_{0.6}Sr_{0.4}Co_{0.2}Fe_{0.8}O_{3-\delta}$ Thin Films. *Appl. Surf. Sci.* **2014**, *323*, 71−77.
(67) Lee, W.; Han, J. W.; Chen, Y.; Cai, Z.; Yildiz, B. Cation Size Mismatch and Charge Interactions drive Dopant Segregation at the Surfaces of Manganite Perovskites. *J. Am. Chem. Soc.* **2013**, *135*, 7909−7925.
(68) Tselev, A.; Vasudevan, R. K.; Gianfrancesco, A. G.; Qiao, L.; Ganesh, P.; Meyer, T. L.; Lee, H. N.; Biegalski, M. D.; Baddorf, A. P.; Kalinin, S. V. Surface Control of Epitaxial Manganite Films via Oxygen Pressure. *ACS Nano* **2015**, *9*, 4316−4327.

DOI: 10.1021/acsaem.8b00586
ACS Appl. Energy Mater. 2018, 1, 4522−4535